International Journal of Minerals, Metallurgy and Materials
Accepted manuscript, https://doi.org/10.1007/s12613-020-2030-3

A simple and novel synthetic route to anatase TiO_2 nanopowder from natural ilmenite via H_3PO_4/NH_3 process

Lalinda Palliyaguru, Ushan S Kulathunga, Lakruwani I Jayarathna, Champa D Jayaweera, and Pradeep M Jayaweera

Dept. of Chemistry, University of Sri Jayewardenepura, Nugegoda-10250, Sri Lanka.

Abstract: A simple and novel technique for the preparation of anatase TiO_2 nanopowder using natural ilmenite ($FeTiO_3$) as the starting material is reported. Digesting ilmenite with concentrated H_3PO_4 under refluxing conditions yields white α-titanium bismonohydrogen orthophosphate monohydrate (TOP), $Ti(HPO_4)_2.H_2O$, which can be easily isolated via gravity separation from unreacted ilmenite. Addition of ammonia to separated TOP followed by calcination at 500 ℃ completes the preparation of anatase TiO_2. Calcination at temperatures above 800 °C converts anatase form of TiO_2 to the more stable phase, rutile. Removal of iron from ilmenite is problematic and environmentally unfriendly in the commercial production of synthetic TiO_2. In the present study, removal of iron was found to be markedly simple due to the high solubility of iron phosphate species in conc. H_3PO_4 with the precipitation of TOP. Titanium content of the prepared samples is over 90% on metal basis having silica and phosphorous as major impurities. Prepared TiO_2 samples were characterized using X-ray fluorescence, FTIR, Raman spectroscopy, UV-visible diffuse reflectance spectroscopy, high-resolution transmission electron microscopy and X-ray diffraction analyses. The photocatalytic potential of commercial and as-prepared titania samples was assessed by photodegradation of rhodamine B dye.

Keywords: ilmenite; phosphoric acid; titanium phosphates; titanium dioxide; anatase; rutile

1. Introduction

Titanium dioxide (TiO_2) is a mineral that occurs in nature as three well-known polymorphs: rutile, anatase, and brookite. Among the three polymorphs, rutile is the most abundant and stable phase [1, 2]. Anatase and brookite are both metastable phases that transform exothermally and irreversibly into rutile phase under heat, pressure, or other conditions. The phase transition [3-6] of anatase to rutile occurs in the temperature range between 350 and 1175 ℃ enabling anatase to be used in technological applications. The crystal structures of

rutile, anatase, and brookite are all based on the distorted TiO_6 octahedral units that share corners and edges in different connections while keeping the overall stoichiometry as TiO_2. Rutile has a straight chain of octahedra linked via corner connections, and anatase has a zigzag chain of octahedra via edge connections. Anatase has more edge sharing octahedra than rutile and therefore, has larger interstitial spaces between the octahedra. The crystal structures of these polymorphs and some known physical properties such as refractive index and density are interconnected [5, 7, 8]. For example, rutile with a higher refractive index makes it a superior pigment [9]. Anatase having a larger band gap makes it more photoactive than rutile. The high photoactivity of anatase has therefore found some applications in solar cells, and photocatalysis [10, 11].

Among many techniques used in the preparation of anatase TiO_2 nanomaterials [12-14], hydrothermal methods have gained much interest due to their relative simplicity, cost effectiveness and varying degrees of chemical/physical properties [15, 16]. According to the previous work, titanium(IV) compounds, mainly but not exclusively $TiCl_4$, and organic titanium have been widely used as the starting material in the preparation of anatase phase [12, 14, 17, 18]. A number of groups have attempted to selectively crystallize anatase or rutile after hydrolysis of $TiCl_4$ through controlling the solution pH, concentration of reactants and the mineralizer [5, 19]. R. Parra *et al.* [20] prepared high purity anatase nanoparticles with diameters ranging from 6 to 30 nm from titanium(IV) isopropoxide and acetic acid. Titanium alkoxide was successfully used in the synthesis of anatase nanomaterials via sol-gel hydrolysis, precipitation and followed by calcination or hydrothermal treatment [18]. Precise control over these laboratory parameters is critical to the phase selectivity. The high sensitivity of $TiCl_4$ and alkoxides to atmospheric moisture is a major disadvantage in industrial production of anatase TiO_2.

Ilmenite ($FeTiO_3$) is the most abundant and most widely used material in the synthesis of titanium compounds that include anatase TiO_2, $TiCl_4$, and organic titanium [21, 22]. Removal of iron, the major impurity in ilmenite is challenging owing to the large quantities of iron present in the ore. This is primarily due to the lack of selectivity between iron and titanium in acid/base dissolution kinetics [21, 23]. Currently, there are two major industrial scale processes for the production of titanium compounds from ilmenite namely, the sulfate and the chloride process [24, 25]. The main feed stocks for these processes are TiO_2 slag and/or synthetic rutile produced from ilmenite ore. The most common method for producing TiO_2 slag is via smelting process in which iron oxides is reduced to liquid iron in an electric arc furnace. Titania slag can be used to produce synthetic rutile, which is a further upgraded raw material with a TiO_2 content of 92–96%. The preparation of synthetic anatase from ilmenite ore involves several additional steps after the synthesis of pure titanium (IV) compounds. For example [26, 27], in recent attempts in the preparation of synthetic anatase by digestion of

ilmenite using two common leaching agents, HCl and H_2SO_4 involved several physical and chemical processing steps. Physical processes like, calcination and mechanical activation of ilmenite prior to the acid leaching and also the use of iron powder and other chemicals like; Na_2S and H_2O_2 make the process commercially less viable in the preparation of anatase TiO_2.

In the present study, we report a simple and novel hydrothermal method for the direct preparation of synthetic anatase from ilmenite through digestion with conc. H_3PO_4 followed by ammonia. The use of ilmenite as the feedstock and absence of additional steps in the iron removal process are the key advantages in this method compared to the majority of other synthetic routes for the synthesis of anatase TiO_2. Additionally, the entire chemical process requires only two industrial chemicals without the involvement of high energy steps like smelting. The solid precipitate of TOP separated from soluble iron complexes after digestion in concentrated phosphoric acid solution was reacted with ammonia to obtain anatase TiO_2. We recently reported [28] the preparation of TOP, a white pigment from ilmenite using 85% H_3PO_4 for possible applications in the field of cosmetic industry. In the present investigation, the same material was used as a precursor for the synthesis of anatase grade titania. Furthermore, rutile phase titania was obtained upon the heat treatment of prepared anatase. The photocatalytic activity of as-prepared titania compounds on rhodamine B (RhB) were assessed and compared with the commercial grade titania samples.

2. Experimental

2.1. Preparation of Anatase/Rutile Nanopowder:

Firstly, TOP was synthesized by digesting 100 g of Hi-Ti ilmenite (Lanka Mineral Sands Limited, Sri Lanka) and 800 ml of 85% H_3PO_4 (Orthophosphoric Acid LR, TECHNO PHARMCHEM) for 5 hours under refluxing condition. The mixture was allowed to cool down and settle into layers at the room temperature. A white precipitate of TOP was settled between most dense layer of unreacted ilmenite in the bottom and the least dense layer of liquid portion rich with iron phosphates on the top (Fig. 1.). Upper two layers were separated mechanically via decantation technique, and unreacted ilmenite remained in the reaction vessel. The separated middle layer rich with TOP was thoroughly mixed with 100 ml of distilled water and allowed to resettle for 24 hrs. This step was repeated for four times until the white portion is free of residual amounts of unreacted ilmenite and H_3PO_4. The identity of TOP was confirmed by XRD and FTIR analysis. Secondly, 200 ml of 25% NH_3 (RESEARCH LAB FINE CHEM INDUSTRIES) was added to 30 g of pure TOP and vigorously stirred for

2 hours at 40 ℃. This step was repeated 4 times and the mixture was allowed to settle at room temperature for 24 hours. The white precipitate was separated and calcined (Box-type resistance furnace SX-2.5-10) at 500 ℃. XRD pattern of the final product confirmed the formation of anatase. Ilmenite samples and all chemicals were used as received without any further purification.

2.2. XRD Analysis.

X-ray diffraction (XRD) patterns of ilmenite, TOP, anatase, and rutile samples were analyzed using XRD instrument (Rigaku Ultima-IV) equipped with Cu Kα source and scintillation detector. Diffractograms were generated by scanning in the 2θ range of 10°-100° with a 0.02° step size and a scan time of 1 sec per step. Prepared titania samples were calcined for 5 hours at the temperatures of 500, 700, 800 and 900 ℃ prior to the XRD analysis. The particle diameter (D) of prepared titania samples were calculated from the most intense diffraction peaks of (101) and (110), for anatase and rutile, respectively, using the Scherrer formula (Eq. 1) [29];

$$D = \frac{0.9\lambda}{\beta Cos(\theta)} \quad (1)$$

where λ is the X-ray wavelength employed, θ is the diffraction angle of the respective peak, and β is defined as the full-width at half maximum of the peak.

The weight percentage of anatase, [A] %, was determined for each calcination temperature using the Spurr equation (Eq. 2) [30]:

$$[A]\% = \frac{100 \times I_A}{I_A + 1.265 \times I_R} \quad (2)$$

Where, I_A and I_R correspond to the areas of the anatase (101) and rutile (110) XRD peaks, respectively. Therefore, rutile percentage is equal to [R]% = 100 - [A]%.

2.3. TEM Analysis.

The morphology of the powder materials was investigated by the high resolution transmission electron microscopy (HR-TEM ZEISS Libra 200 Cs-TEM) at an accelerating voltage of 200 kV. TEM images of the titania samples were obtained after calcining at 700 and 900 ℃ , respectively. Particle sizes were analyzed using the ImageJ software.

2.4. Raman Spectroscopy.

Raman spectra of TiO_2 samples were obtained with Bruker Senterra Raman spectrometer with the laser excitation wavelength of 785 nm and incident power of 10 mW. Aperture size of 25×1000 μm and integration time of 5 s were chosen during the data collection.

2.5. XRF analysis.

The chemical composition of samples was analyzed by XRF. HORIBA Scientific XGT- 5200 X-ray Analytical Microscope equipped with a Rh anode X-ray tube operated at maximum voltage of 50 kV and current of 1 mA with a peltier cooled silicon drift detector.

2.6. UV-Vis diffuse reflectance spectroscopy.

UV-Vis diffuse reflectance spectra (UV-Vis DRS) of the powder samples were measured using a PerkinElmer Lambda 35 spectrometer. UV-Vis DRS were obtained with 1.25-inch calibrated certified reflectance standard (SRS-99-010) as the background equipped with a 50-mm integrating sphere. The optical reflectance was measured in the 300–900 nm range.

UV-Vis absorbance spectroscopy coupled with Kubelka–Munk method [31] was used to evaluate the band gap energies of prepared anatase and rutile TiO_2. Kubelka–Munk method is based on the following equation,

$$F(R) = \frac{(1-R)^2}{2R} = \frac{\alpha}{s} \quad (3)$$

where *F(R)* is Kubelka–Munk function, *R* the reflectance, s is the scattering factor and α is the absorption coefficient. The modified Kubelka-Munk function can be expressed as follows;

$$[F(R) \times hv]^n \quad (4)$$

where n is associated with the electronic transition. $n = {}^{1}/_{2}$ for an indirect allowed transition and $n = 2$ for a direct allowed transition.

2.7. Photocatalytic degradation of rhodamine B.

Photocatalytic activities of prepared titania samples were tested via bleaching a sample of rhodamine b (Loba Chemie) dissolved in 50.00 ml of distilled water under UV irradiation (250 W Hg arc Philips UV Lamp). In a typical experiment, a sample of 150.0 ml dye solution loaded with 0.10 g TiO_2 was exposed to UV light. All the photocatalytic tests were conducted by stirring the suspension with a magnetic stirrer. Before irradiating, all samples were stored in the dark for 20 minutes in order for the samples to reach the sorption equilibrium. After being illuminated for certain period of time, a sample of the suspension was centrifuged at 5000 rpm for 20 min to get a clear separation of the liquid portion. The concentration of the RhB in the solution was determined through UV-Vis spectroscopy by measuring absorbance (Perkin-Elmer Lambda 35) at 554 nm. Commercial anatase TiO_2 sample (MERCK, K19722608) was used for comparison. Pigment grade TiO_2 (Brand Ti-Pure^{TM}) was used as the commercial rutile.

3. Results and discussion

3.1. Preparation of anatase/rutile TiO_2.

The flowchart for the preparation of anatase/rutile TiO_2 from the starting material ilmenite is shown in Fig. 1. The XRD and SEM images of the ilmenite sample are shown in Fig. 2. The average particle size of the ilmenite samples as received was around 100 ±25 µm. Table 1 shows the metal oxide composition of the ilmenite sample analyzed by X-ray fluorescence (XRF) technique. A series of leaching experiments under refluxing condition were conducted with different volume to mass ratios between 85% H_3PO_4 and ilmenite. The white precipitate formed in the ilmenite/H_3PO_4 digestion mixture was confirmed as α-titanium bismonohydrogen orthophosphate monohydrate (TOP) with chemical formula $Ti(HPO_4)_2.H_2O$ by the XRD analysis (Fig. 3a.) and it matches with the ICDD DB Card No. 01-080-1067. The FTIR spectrum further confirms the formation of TOP [32, 33] (Supporting Information, Fig. S1.). The optimum ilmenite phosphoric acid mass to volume ratio (g:ml) was chosen to be 1:8 based on the maximum yield of the product TOP formed and the minimum residual weight of unreacted ilmenite. Lower mass/volume ratios produced lower weight percentages of TOP. Dry weights of TOP and unreacted ilmenite were measured after washing thoroughly with distilled water. Weight of the TOP

precipitate reached to its maximum level approximately after 5 hrs. of refluxing (*see* Supporting Information, Table S1). About 20 g of TiO_2 was obtained when 100 g of ilmenite was used as the starting material and the consumption of water and ammonia is 500 and 800 ml, respectively. The calculated recovery of titanium is about 35-40 percent under our experimental conditions. A detailed description for the preparation of titanium phosphates from natural ilmenite was reported by our group in a recent article [28].

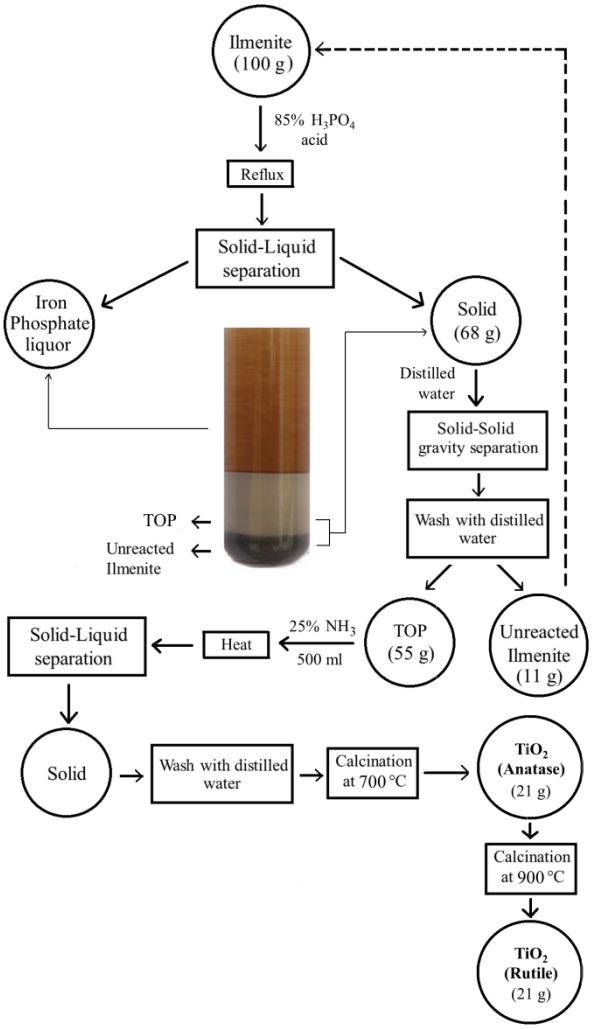

Fig. 1. Flowchart for the preparation of TiO_2 from ilmenite.

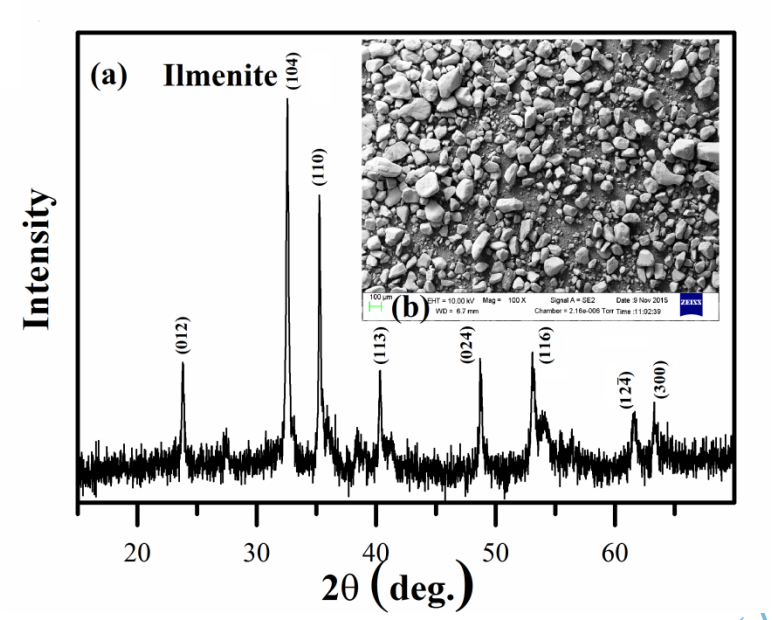

Fig. 2. XRD pattern (a) and SEM image (b) of ilmenite.

Table 1. Metal oxide percent composition of ilmenite and anatase TiO_2.

Material	TiO_2	Fe as FeO	P as Phosphates	CaO	SiO_2	SnO	ZnO	S as sulfates	MnO_2	ZrO_2	Nb_2O_5	Cr_2O_3	Al_2O_3
Ilmenite ($FeTiO_3$)	66.97	28.66	-	0.31	1.20	0.23	0.02	-	0.80	0.15	0.26	0.55	0.85
Anatase (TiO_2)	88.21	0.20	2.36	0.79	8.17	0.08	0.05	0.14	-	-	-	-	-

One of the key successes in the preparation of synthetic TiO_2 from ilmenite reported in this study is the ability to prepare an iron free titanium phosphate compound, i.e. TOP that can be used as the precursor for the preparation of both anatase and rutile TiO_2. Titanium which is in its 4+ oxidation state in natural ilmenite are consumed during H_3PO_4 digestion for the formation of insoluble $Ti(HPO_4)_2{\cdot}H_2O$, whereas iron mainly in its 2+ oxidation state leach to the liquid phase to form the soluble $Fe(H_2PO_4)^+$ in conc. H_3PO_4. Ratanatamskul *et al.* [34] has reported at pH < 3 H_3PO_4 with Fe(II) forms soluble $Fe(H_2PO_4)^+$ species as $H_2PO_4^-$ dominates in acidic conditions. The equation (5) explains the formation of both TOP and iron(II) phosphate complex. Further, oxidation of Fe(II) to Fe(III) takes place at elevated temperatures and highly soluble iron(III) complexes are formed in concentrated H_3PO_4. Therefore, leaching of iron from ilmenite in to concentrated H_3PO_4 is less problematic as a result of the formation of multi-ligand complexes of both iron(II)/(III) with phosphate such as

$Fe(H_2PO_4)^+$, $Fe(H_2PO_4)^{2+}$, $FeH_5(PO_4)_2^{2+}$ and $FeH_7(PO_4)^{3+}$ which are highly soluble in concentrated H_3PO_4 as reported in several studies [34-37]. The chemical reaction for the iron dissolution and TOP precipitation in concentrated phosphoric acid can be proposed according to the following equation;

$$FeTiO_3(s) + 10H^+(aq) + 3PO_4^{3-}(aq) = Ti(HPO_4)_2(s) + Fe(H_2PO_4)^+(aq) + 3H_2O(l) \quad (5)$$

Further, we have not attempted to understand the complexes of iron phosphates that leached in to phosphoric acid, instead emphasis was given to the solid fraction that has resulted after acid digestion. Iron phosphates in the H_3PO_4 liquor could be used in many applications, such as an ingredient in fertilizer, pesticide and paint industries. Moreover, to confirm that iron is leaching in to H_3PO_4, an experiment was performed by gradually adding the leachate into cold acetone to obtain a white precipitate which was isolated and calcined at 500 °C for 5 hrs. XRD analysis confirms that material isolated as $Fe(PO_3)_3$ (Supporting Information, Fig. S2.) which matches with the previously published work [38].

The white precipitate TOP, free of both residual iron and H_3PO_4 after washing with distilled water was reacted with ammonia (Eq. 6) to obtain a precipitate of $Ti(OH)_4$, which was then thermally decomposed to form the final product TiO_2 (Eq. 7).

$$Ti(HPO_4)_2(s) + 4NH_4OH(aq) \rightarrow Ti(OH)_4(s) \downarrow + 2(NH_4)_2HPO_4(aq) \quad (6)$$

$$Ti(OH)_4(s) \xrightarrow{\Delta} TiO_2(s) + H_2O(l) \quad (7)$$

The removal of PO_4^{3-} from solid TOP when reacted with ammonia increases the PO_4^{3-} concentration in the aqueous ammonia phase as $(NH_4)_2HPO_4$ resulting a decrease of PO_4^{3-} in the solid phase. The concentration of PO_4^{3-} in the liquid phase was measured against the number of washes of solid TOP and it clearly indicates that PO_4^{3-} concentration decreases with number of washes (Supporting Information, Figure S3). It is apparent that PO_4^{3-} reached to an undetectable level after the fourth wash. Removal of PO_4^{3-} is a result of the formation of highly water soluble ammonium phosphate salts in the presence of conc. ammonia. Further, reaction of TOP

with ammonia forms a fine white colloidal suspension which takes fairly long time to settle down, a clear indication for the formation of titanium hydroxide. The calcination of this white precipitate for 5 hours at 700 ℃ developed a white powder characteristic to nano level anatase TiO_2, which was confirmed by the XRD (Fig. 3b) (ICDD DB Card No. 01-084-1285) analysis.

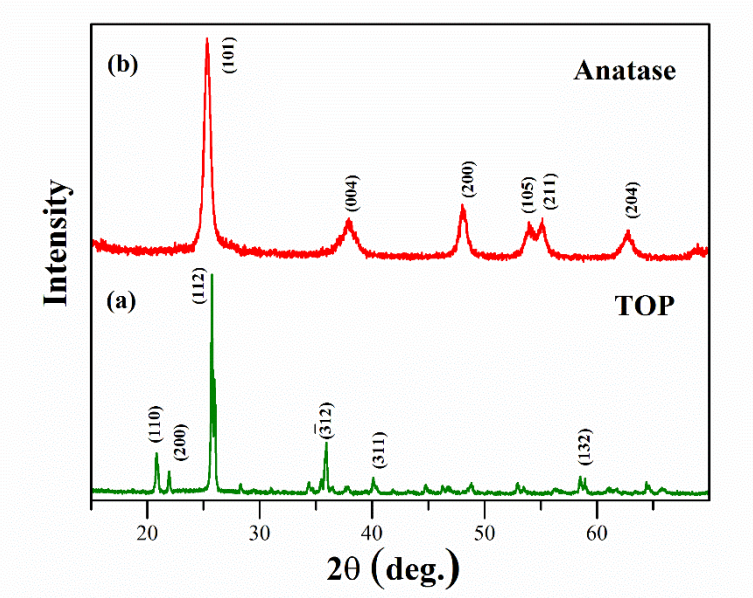

Fig. 3. XRD patterns of (a) TOP and (b) antase TiO_2.

3.2. XRD and TEM analyses of TiO_2.

XRD patterns of the prepared titania samples were recorded after 5 hours of calcination at temperatures of 500, 700, 800 and 900 ℃ (Fig. 4). Fig. 4a shows the XRD pattern of sample calcined at 500 ℃, indicating the presence of anatase phase with broad XRD peaks. At 700 ℃, characteristic XRD peaks of anatase emerged with 2θ values centered at 25.31, 37.80, 48.04, 53.89, 55.06, and 62.69 corresponding to the crystal planes (101), (004), (200), (105), (211), and (204), respectively. XRD pattern is in good agreement with the XRD pattern observed for commercial anatase sample. The calculated particle sizes based on Scherrer formula (Eq. 1) [29] and the calculated anatase percentages based on Spurr equation (Eq. 2) [30] at different temperatures are summarized in Table 2. The calculated particle size for anatase at 700 ℃ is 11.4 nm and this was further confirmed by the TEM images (Fig. 5.) of the same sample. The XRD pattern obtained for the sample calcined at 800 ℃ (Fig. 4c) indicates the presence of rutile crystal planes (110), (101), (200), (111), (210), (211), (220), (002) and (310) corresponding 2θ values of 27.44. 36.08, 39.20, 41.24, 44.06, 54.33, 56.64, 62.75 and 64.07,

respectively, in addition to typical anatase diffraction peaks. The presence of diffraction peaks characteristic to both anatase and rutile phases indicates the phase transformation from anatase to rutile takes place at around 800 ℃. The calculated anatase percentage in the sample calcined at 800 ℃ is about 70% (Table 2). The calculated particle size at 800 ℃ for TiO_2 is 20.9 nm, as the transformation to rutile is accompanied by a significant grain growth (Supporting Information, Fig. S4.) [39]. A complete transition to rutile was evident at 900 ℃ with the emergence of characteristic XRD pattern for rutile (Fig. 4d.). The transition temperature for anatase to rutile can be significantly affected by several factors such as the presence of cationic and anionic impurities [40, 41], grain size [42], and reaction atmosphere [43]. Furthermore, a stark effect of silica additive on the anatase to rutile phase transition has been observed [44]. Therefore, the presence of a significant amount of SiO_2 (~8 %) in the synthesized anatase can be the primary reason for the observed higher temperature for anatase to rutile phase transition in this study. The calculated particle size for rutile is about 41.5 nm. XRD patterns of commercial anatase and rutile samples used in this work are shown in Supporting Information, Fig. S5. The morphological characterization was performed by analyzing TEM images for the prepared anatase TiO_2 samples (Fig. 5). The average particle size based on TEM image analysis is in the range 11±4 nm for the prepared anatase samples. Further, TEM images suggest that TiO_2 nanoparticles are more special in shape.

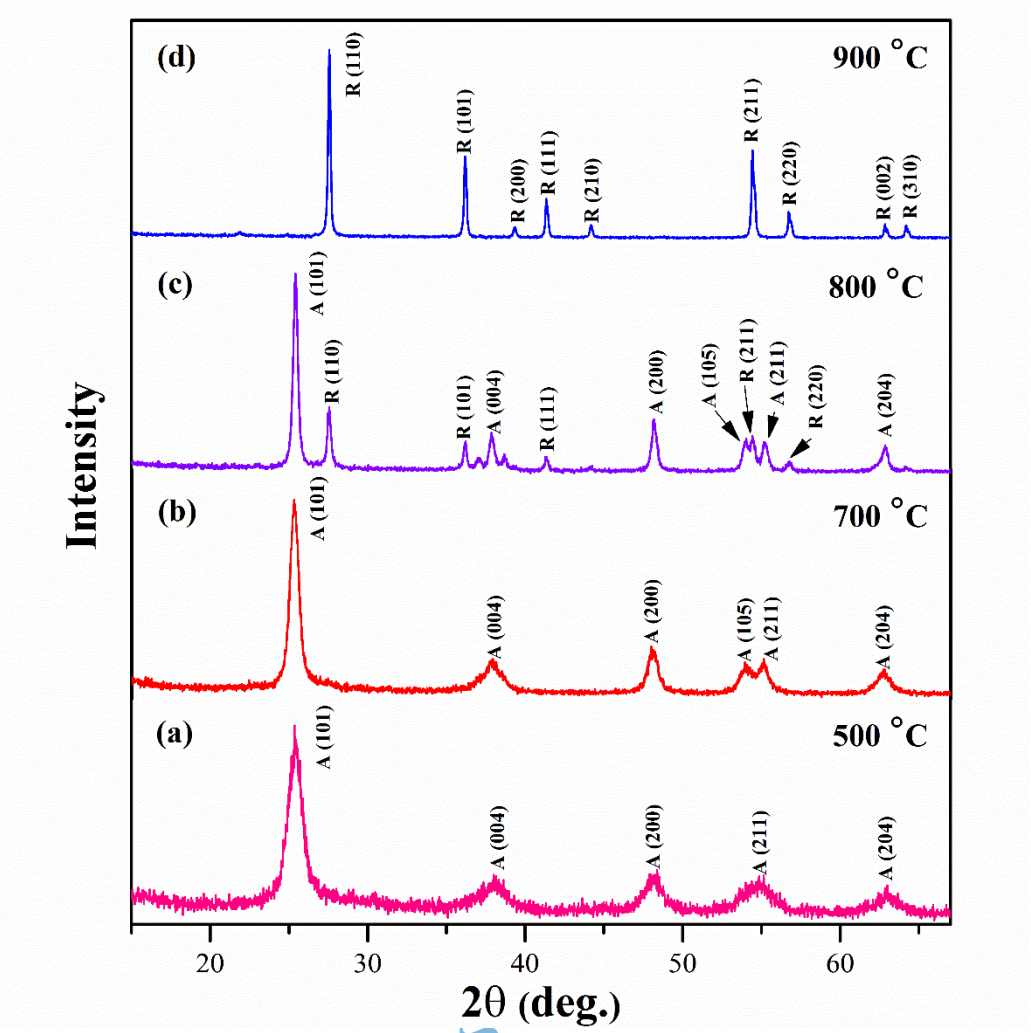

Fig. 4. XRD patterns of as-prepared TiO_2 sample calcined at different temperatures.

Table 2. Particle size and anatase percentage calculated for prepared TiO_2 samples at different calcination temperatures.

Temperature / °C	Particle size / nm	Anatase / wt%
700	11.4	~100
800	20.9	~70
900	41.5	0

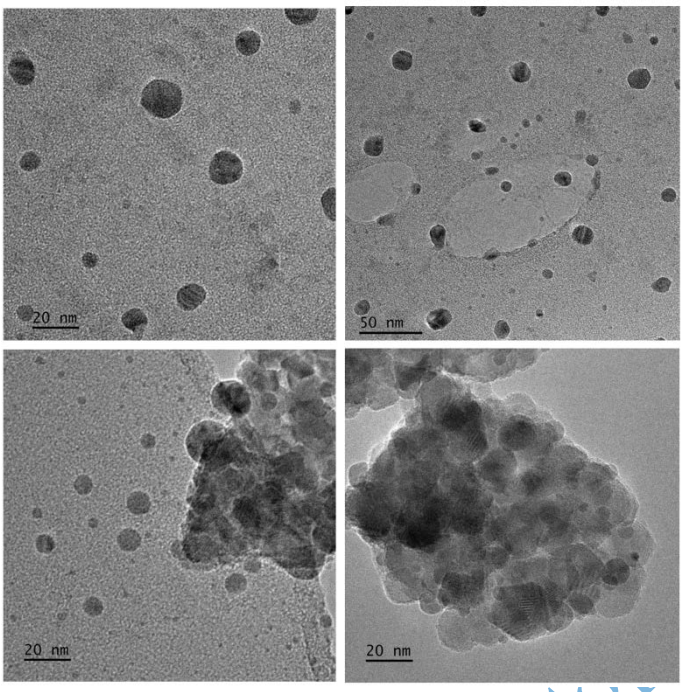

Fig. 5. HR-TEM images of anatase TiO_2 nanopowder.

3.3. Raman analysis.

Raman spectroscopy is a useful tool in the analysis of TiO_2 polymorphs as they exhibit characteristic Raman bands [7, 45, 46]. Different arrangements of the same fundamental structural unit of [TiO_6] octahedron in rutile and anatase make them belong to different space groups. Anatase belongs to the space group of $D_{4h}^{19} = I4_1/amd$ with $Z = 4$ and has the irreducible representation for the optical modes:

$$\Gamma_{opt} = A_{1g}(R) + 2B_{1g}(R) + 3E_g(R) + B_{2u}(ia) + A_{2u}(IR) + 2E_u(IR)$$

Therefore, anatase has six Raman active modes. Rutile belongs to the space group of $D_{4h}^{14} = P4_2/mnm$ with $Z = 2$ and has the irreducible representation for the optical modes:

$$\Gamma_{opt} = A_{1g}(R) + A_{2g}(ia)_g + B_{1g}(R) + B_{2g}(R) + E_g(R) + A_{2u}(IR) + 2B_{1u}(ia) + 3E_u(IR).$$

Therefore, rutile has four Raman active modes. Fig. 6a shows the Raman spectrum of anatase prepared after calcination at 700 ℃ for 5 hours. The Raman spectrum of anatase is featured with a strong and sharp band at 144 cm^{-1}, three mid-intensity bands at 396, 515, and 638 cm^{-1}, and a weak and low intensity band at 197 cm^{-1}. Superposition of two fundamental bands at 515 cm^{-1} makes the appearance of six Raman bands for anatase corresponding to the symmetries of E_g, E_g, B_{1g}, A_{1g}, B_{1g}, and E_g, respectively. The Raman spectrum of prepared anatase is in good agreement with previously reported data [6, 46], which further confirms the chemical identity of prepared anatase TiO_2 in this work. As it was evident by XRD analysis, a complete transformation of anatase to rutile has taken place after calcination at 900 ℃ for 5 hours. Fig. 6b shows the Raman spectrum of prepared rutile sample, featuring with two strong bands, at 443, 608 cm^{-1}, and a weak band at 143 cm^{-1} corresponding to E_g, A_{1g}, and B_{1g}, respectively. The broad and mid-intensity peak at 238 cm^{-1} is a result of two-photon scattering of rutile. The XRD and Raman spectral data are in good mutual agreement and provide strong experimental evidences for the preparation of anatase and rutile from ilmenite/H_3PO_4 digestion.

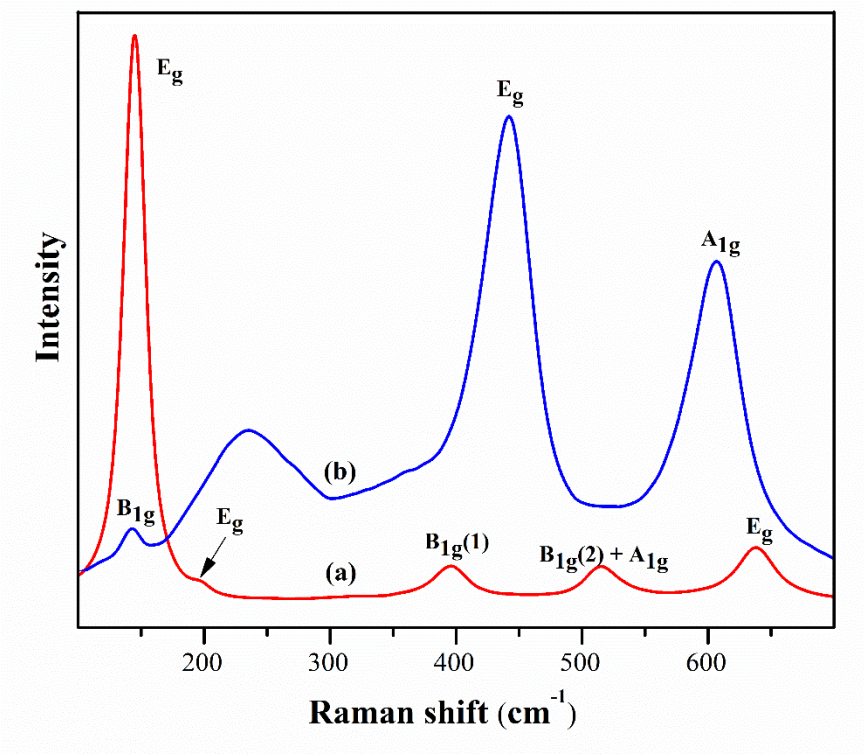

Fig. 6. Raman spectra of prepared (a) anatase (b) rutile TiO_2 samples.

3.4. XRF analysis.

The XRF analysis showed that the titanium oxide content has enhanced to 88.2 % (Ti metal basis 90.6 % in the prepared TiO_2 from 66.9 % in ilmenite (Table 1). Trace metals, Mn, Zr, Nb, Cr, and Al in ilmenite are absent in the final product TiO_2. A low iron oxide content of 0.2 % in anatase samples further confirms an effective removal of iron through the digestion of ilmenite with conc. H_3PO_4. The presence of phosphorous in the phosphate form by 2.4 % may be the result of insoluble metal phosphates such as calcium and silicon phosphates [47] arising from H_3PO_4 digestion. In general, phosphoric acid (85% w/w) has several anionic impurities [48] such as SO_4^{2-}, and SiO_2^-. The presence of 0.14 % sulfur, assumed to be in the sulfate form in the final product may have resulted from the phosphoric acid. Further, silicon, an impurity in both natural ilmenite and H_3PO_4 could be the main reason for 8.2 % silicon assumed to be in the oxide form in the final product.

3.5. Optical Properties.

UV-Vis diffuse reflectance spectra (UV-Vis DRS) of the prepared anatase and rutile TiO_2 samples are shown in Fig. 7. Absorption edges for anatase and rutile samples are located at 384 and 412 nm, respectively in the UV-Vis absorption spectrum calculated from diffuse reflectance (Supporting Information, Fig. S6) data using the Kubelka–Munk method [31, 49]. According to literature [50], anatase is an indirect transition semiconductor, whereas rutile is a direct transition semiconductor. The plotting of $[F(R) \times h\nu]^n$ as a function of photon energy, E_{phot}, (*Insert* of Fig. 7) was used to obtain the band gap energy, which corresponds to the value of E_{phot} extrapolated to $\alpha = 0$, where *F(R)* is the Kubelka–Munk function. Calculated band gap energies of anatase and rutile are 3.09 and 2.95 eV, respectively. The values are in the range of the reported values in literature [51, 52]. However, the theoretical band gap values reported for anatase and rutile are 3.2 and 3.0 eV, respectively, which are higher than the band gap values obtained for the prepared anatase and rutile. The presence of metallic and non-metallic impurities (Table 1) in the final product may have a significant effect on the shift of band gap from the original value due to factors such as oxygen vacancy, and lattice disorientations, which affect the electronic transition from valance to conduction band [53]. For example, Karbassi *et al.* [54] have reported the presence of SiO_2 and Fe oxide in the titania matrix leading to a significant red shift of optical response towards the visible light owing to the reduced band gap energy.

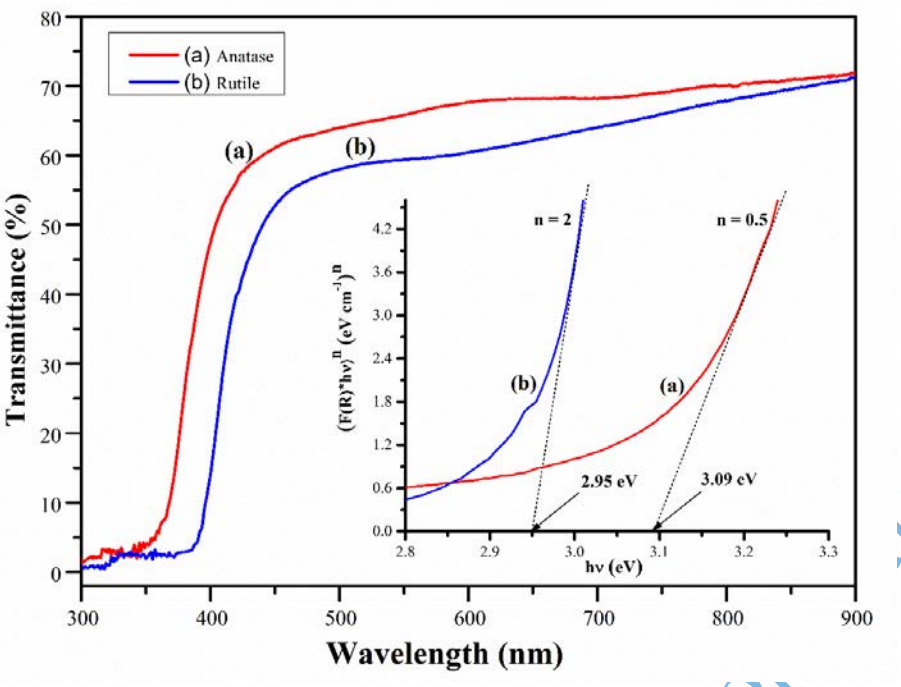

Fig. 7. UV-Vis diffuse reflectance spectra of (a) anatase and (b) rutile TiO_2 samples. *Inserted*: Band gap curves.

3.6. **Photocatalytic degradation of organic dyes.**

The photocatalytic properties of TiO_2 originate from the formation of photogenerated charge carriers (holes and electrons) which generate after the absorption of ultraviolet (UV) light corresponding to the band gap. The photogenerated holes in the valence band diffuse to the TiO_2 surface and react with adsorbed water molecules to form hydroxyl radicals. The photogenerated holes and the hydroxyl radicals oxidize organic molecules adsorbed to the TiO_2 surface. Meanwhile, electrons in the conduction band also participate in reduction processes by reacting with molecular oxygen to produce superoxide radical anions. The superoxide radical ions are highly reactive and can subsequently breakdown the organic molecules present in the solution [55-58]. The photodegradation (Supporting Information, Fig. S7.) kinetics of RhB for titania and ilmenite samples were investigated by pseudo-first order method of Langmuir-Hinshelwood model [59] (Eq. 8), which is a well-established method for heterogeneous catalysis at low dye concentration. According to this model,

$$\ln\left(\frac{C_0}{C_t}\right) = kt \qquad (8)$$

where C_0 is the initial dye concentration, C_t is the dye concentration after UV irradiation time of 't', and k is the pseudo first order rate constant (min^{-1}). k values were graphically determined using the regression method. Half-life, $t_{1/2}$, which is the time required for 50% reduction of the dye concentration, was calculated by the following equation:

$$t_{1/2} = \frac{\ln 2}{k} = \frac{0.6931}{k} \quad (9)$$

The photocatalytic activity of as-prepared anatase, rutile, and commercially available anatase and rutile samples on degradation kinetics of rhodamine B are shown in Fig. 8. Estimated rate constant k, and $t_{1/2}$ (Eq. 8 and 9) values for kinetic experiments are listed in Table 3.

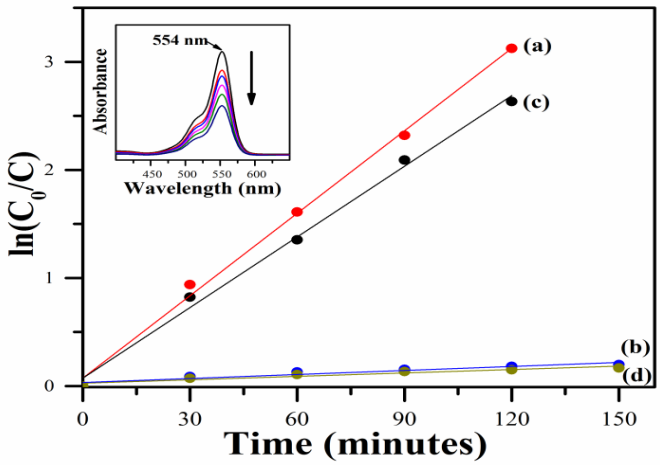

Fig. 8. Photocatalytic degradation kinetics of RhB dye over (a) prepared anatase, (b) prepared rutile, (c) commercial anatase and (d) commercial rutile TiO_2 samples. *Inserted*: Typical UV-Vis absorption decay at different time intervals.

Table 3. Rate constants of degradation kinetics for RhB dye over titania samples.

Material	$k \times 10^3$ / min^{-1}.	$t_{1/2}$ / min.	R^2
Anatase	25.4	27.3	0.9959
Rutile	1.24	559	0.8871
Commercial Anatase	21.8	32.8	0.9934
Commercial Rutile	1.05	660	0.8953

Photobleaching of RhB was not observed for control experiments performed using starting material, ilmenite in the presence and absence of UV light. Further, adsorption capacities are negligible for all samples and the results are in agreement with the previously published work [60]. Both prepared and the commercial anatase samples behaved almost identically for the RhB photodegradation giving similar rate constants of 25.4×10^{-3} min^{-1} and 21.8×10^{-3} min^{-1}, respectively. Hence, it is clear that prepared anatase in this work has the same photocatalytic potential as the commercial anatase used in our experiments. Rate constants for as-prepared rutile the values is 1.24×10^{-3} min^{-1} whereas, for commercial rutile 1.05×10^{-3} min^{-1}. Both commercial and prepared rutile samples are having average particle size close to 100 nm. It is generally accepted that higher phase pure anatase exhibits higher photocatalytic activity due to large band gap, surface and charge transport properties [61]. Similar photodegradation kinetics observed for both prepared and commercial samples may be due to the lower percentage of metallic impurities such as iron, which could change the photobleaching rate. Presence of Si, P and Ca impurities appeared to have no major influence on the kinetic parameters.

4. Conclusions

We have successfully prepared anatase TiO_2 nanopowder by employing a simple and novel ilmenite/H_3PO_4 digestion route. The precipitation of iron free titanium complex, i.e. α-titanium bismonohydrogen orthophosphate monohydrate (TOP) in the H_3PO_4 leachate, which can be easily isolated from soluble iron in the form of iron-phosphate complexes, provides the key advantage of preparing a high purity titanium precursor complex for anatase preparation. Repeated washing of TOP with ammonia not only form titanium hydroxide but also remove the phosphate from the solid. The role of the calcination temperature on prepared anatase was investigated from 500 - 900 °C and it showed that the anatase to rutile transformation starts to take place above 700 °C. The chemical identity of prepared TiO_2 samples was confirmed by Raman and XRD data. Metal oxide content obtained via XRF data indicates that prepared TiO_2 samples are having 88% TiO_2. The photocatalytic performance of the as-prepared anatase and commercial anatase exhibits similar results on the photodegradation kinetics of rhodamine B.

Acknowledgements

This work was financially supported by University of Sri Jayewardenepura with the grant number ASP/01/RE/SCI/2019/31. The authors also thank Lanka Mineral Sands Ltd, Sri Lanka for providing ilmenite

samples, Central Instrument Facility of the University of Sri Jayewardenepura for XRD sample analysis and Sri Lanka Institute of Nanotechnology (SLINTEC) Analytical Service for Raman, TEM and XRF analyses.

References

[1] A. F. Wells, *Structural Inorganic Chemistry*, OUP Oxford, 2012.

[2] N. N. Greenwood and A. Earnshaw, *Chemistry of the Elements*, Elsevier Science, 2012.

[3] X.-Z. Ding, X.-H. Liu and Y.-Z. He, Grain size dependence of anatase-to-rutile structural transformation in gel-derived nanocrystalline titania powders, *Journal of Materials Science Letters*, 15(1996), No.20, p.1789.

[4] K. Sabyrov, N. D. Burrows and R. L. Penn, Size-Dependent Anatase to Rutile Phase Transformation and Particle Growth, *Chemistry of Materials*, 25(2013), No.8, p.1408.

[5] J.-G. Li, T. Ishigaki and X. Sun, Anatase, Brookite, and Rutile Nanocrystals via Redox Reactions under Mild Hydrothermal Conditions: Phase-Selective Synthesis and Physicochemical Properties, *The Journal of Physical Chemistry C*, 111(2007), No.13, p.4969.

[6] D. A. H. Hanaor and C. C. Sorrell, Review of the anatase to rutile phase transformation, *Journal of Materials Science*, 46(2011), No.4, p.855.

[7] G. A. Tompsett, G. A. Bowmaker, R. P. Cooney, J. B. Metson, K. A. Rodgers and J. M. Seakins, The Raman spectrum of brookite, TiO2 (Pbca, Z = 8), *Journal of Raman Spectroscopy*, 26(1995), No.1, p.57.

[8] J. S. Chen, Y. L. Tan, C. M. Li, Y. L. Cheah, D. Luan, S. Madhavi, F. Y. C. Boey, L. A. Archer and X. W. Lou, Constructing Hierarchical Spheres from Large Ultrathin Anatase TiO2 Nanosheets with Nearly 100% Exposed (001) Facets for Fast Reversible Lithium Storage, *Journal of the American Chemical Society*, 132(2010), No.17, p.6124.

[9] X. Chen and S. S. Mao, Titanium Dioxide Nanomaterials: Synthesis, Properties, Modifications, and Applications, *Chemical Reviews*, 107(2007), No.7, p.2891.

[10] A. L. Linsebigler, G. Lu and J. T. Yates, Photocatalysis on TiO2 Surfaces: Principles, Mechanisms, and Selected Results, *Chemical Reviews*, 95(1995), No.3, p.735.

[11] M. R. Hoffmann, S. T. Martin, W. Choi and D. W. Bahnemann, Environmental Applications of Semiconductor Photocatalysis, *Chemical Reviews*, 95(1995), No.1, p.69.

[12] H. G. Yang, G. Liu, S. Z. Qiao, C. H. Sun, Y. G. Jin, S. C. Smith, J. Zou, H. M. Cheng and G. Q. Lu, Solvothermal Synthesis and Photoreactivity of Anatase TiO2 Nanosheets with Dominant {001} Facets, *Journal of the American Chemical Society*, 131(2009), No.11, p.4078.

[13] D. P. Macwan, P. N. Dave and S. Chaturvedi, A review on nano-TiO2 sol–gel type syntheses and its applications, *Journal of Materials Science*, 46(2011), No.11, p.3669.

[14] F. Bosc, A. Ayral, P.-A. Albouy and C. Guizard, A Simple Route for Low-Temperature Synthesis of Mesoporous and Nanocrystalline Anatase Thin Films, *Chemistry of Materials*, 15(2003), No.12, p.2463.

[15] W. F. SULLIVAN and S. S. COLE, Thermal Chemistry of Colloidal Titanium Dioxide, *Journal of the American Ceramic Society*, 42(1959), No.3, p.127.

[16] H. Cheng, J. Ma, Z. Zhao and L. Qi, Hydrothermal Preparation of Uniform Nanosize Rutile and Anatase Particles, *Chemistry of Materials*, 7(1995), No.4, p.663.

[17] G. Li, L. Li, J. Boerio-Goates and B. F. Woodfield, High Purity Anatase TiO2 Nanocrystals: Near Room-Temperature Synthesis, Grain Growth Kinetics, and Surface Hydration Chemistry, *Journal of the American Chemical Society*, 127(2005), No.24, p.8659.

[18] C.-C. Wang and J. Y. Ying, Sol−Gel Synthesis and Hydrothermal Processing of Anatase and Rutile Titania Nanocrystals, *Chemistry of Materials*, 11(1999), No.11, p.3113.

[19] S. Cassaignon, M. Koelsch and J.-P. Jolivet, Selective synthesis of brookite, anatase and rutile nanoparticles: thermolysis of TiCl4 in aqueous nitric acid, *Journal of Materials Science*, 42(2007), No.16, p.6689.

[20] R. Parra, M. S. Góes, M. S. Castro, E. Longo, P. R. Bueno and J. A. Varela, Reaction Pathway to the Synthesis of Anatase via the Chemical Modification of Titanium Isopropoxide with Acetic Acid, *Chemistry of Materials*, 20(2008), No.1, p.143.

[21] W. Zhang, Z. Zhu and C. Y. Cheng, A literature review of titanium metallurgical processes, *Hydrometallurgy*, 108(2011), No.3, p.177.

[22] K. K. Sahu, T. C. Alex, D. Mishra and A. Agrawal, An overview on the production of pigment grade titania from titania-rich slag, *Waste Management & Research*, 24(2006), No.1, p.74.

[23] L. Palliyaguru, N. D. H. Arachchi, C. D. Jayaweera and P. M. Jayaweera, Production of synthetic rutile from ilmenite via anion-exchange, *Mineral Processing and Extractive Metallurgy*, 127(2018), No.3, p.169.

[24] T. A. Lasheen, Sulfate digestion process for high purity TiO2 from titania slag, *Frontiers of Chemical Engineering in China*, 3(2009), No.2, p.155.

[25] T. Hisashi, N. Eiichi, T. Hitoshi, A. Masahiro and O. Taijiro, Manufacture of High Pure Titanium(IV) Oxide by the Chloride Process. I. Kinetic Study on Leaching of Ilmenite Ore in Concentrated Hydrochloric Acid Solution, *Bulletin of the Chemical Society of Japan*, 55(1982), No.6, p.1934.

[26] S. Sariman, Y. K. Krisnandi and B. Setiawan, Anatase TiO2 Enrichment from Bangka Ilmenite (FeTiO3) and its Photocatalytic Test on Degradation of Congo Red, *Advanced Materials Research*, 789(2013), p.538.

[27] S. Wahyuingsih, A. H. Ramelan, E. Pramono, A. D. Sulistya, P. R. Argawan, F. D. Dharmawan, L. Rinawati, Q. A. Hanif, E. Sulistiyono and F. Firdiyono, Synthesis of anatase and rutile TiO2 nanostructures from natural ilmenite, *AIP Conference Proceedings*, 1710(2016), No.1, p.030023.

[28] L. Palliyaguru, M. U. S. Kulathunga, K. G. U. R. Kumarasinghe, C. D. Jayaweera and P. M. Jayaweera, Facile Synthesis of Titanium Phosphates from Ilmenite Mineral Sand: Potential White Pigments for Cosmetic Applications, *J Cosmet Sci*, 70(2019), No.3, p.149.

[29] B. D. Cullity, *Elements of X-ray Diffraction*, Addison-Wesley Publishing Company, 1978.

[30] R. A. Spurr and H. Myers, Quantitative Analysis of Anatase-Rutile Mixtures with an X-Ray Diffractometer, *Analytical Chemistry*, 29(1957), No.5, p.760.

[31] P. Kubelka, New Contributions to the Optics of Intensely Light-Scattering Materials. Part I, *J. Opt. Soc. Am.*, 38(1948), No.5, p.448.

[32] A. Stoch, W. Jastrzębski, A. Brożek, J. Stoch, J. Szaraniec, B. Trybalska and G. Kmita, FTIR absorption–reflection study of biomimetic growth of phosphates on titanium implants, *Journal of Molecular Structure*, 555(2000), No.1, p.375.

[33] T. S. Sysoeva, E. A. Asabina, V. I. Pet'kov and V. S. Kurazhkovskaya, Alkali (alkaline-earth) metal, aluminum, and titanium complex orthophosphates: Synthesis and characterization, *Russian Journal of Inorganic Chemistry*, 54(2009), No.6, p.829.

[34] C. Ratanatamskul, S. Chintitanun, N. Masomboon and M.-C. Lu, Inhibitory effect of inorganic ions on nitrobenzene oxidation by fluidized-bed Fenton process, *Journal of Molecular Catalysis A: Chemical*, 331(2010), No.1, p.101.

[35] T. Zhang, Y. Lu and G. Luo, Effects of temperature and phosphoric acid addition on the solubility of iron phosphate dihydrate in aqueous solutions, *Chinese Journal of Chemical Engineering*, 25(2017), No.2, p.211.

[36] J. J. Beltrán, F. J. Novegil, K. E. García and C. A. Barrero, On the reaction of iron oxides and oxyhydroxides with tannic and phosphoric acid and their mixtures, Berlin, Heidelberg, 2009, 133.

[37] M. Iuliano, L. Ciavatta and G. De Tommaso, On the Solubility Constant of Strengite, *Soil Science Society of America Journal*, 71(2007), No.4, p.1137.

[38] W. Zhou, W. He, X. Zhang, J. Liu, Y. Du, S. Yan, X. Tian, X. Sun, X. Han and Y. Yue, Simple and Rapid Synthesis of Fe(PO3)3 by Microwave Sintering, *Journal of Chemical & Engineering Data*, 54(2009), No.7, p.2073.

[39] Y.-H. Zhang and A. Reller, Phase transformation and grain growth of doped nanosized titania, *Materials Science and Engineering: C*, 19(2002), No.1, p.323.

[40] W. F. Sullivan and J. R. Coleman, Effect of sulphur trioxide on the anatase-rutile transformation, *Journal of Inorganic and Nuclear Chemistry*, 24(1962), No.6, p.645.

[41] J. Yang and J. M. F. Ferreira, On the Titania Phase Transition by Zirconia Additive in a Sol-Gel-Derived Powder, *Materials Research Bulletin*, 33(1998), No.3, p.389.

[42] X. Z. Ding, X. H. Liu and Y. Z. He, Grain size dependence of anatase-to-rutile structural transformation in gel-derived nanocrystalline titania powders, *Journal of Materials Science Letters*, 15(1996), No.20, p.1789.

[43] K. J. D. Mackenzie, The Calcination of Titania. VI. The Effect of Reaction Atmosphere and Electric Fields on the Anatase-Rutile Transformation, *Trans. J. Brit. Ceram. Soc.*, 74(1975), p.121.

[44] K. Okada, N. Yamamoto, Y. Kameshima, A. Yasumori and K. J. D. MacKenzie, Effect of Silica Additive on the Anatase-to-Rutile Phase Transition, *Journal of the American Ceramic Society*, 84(2001), No.7, p.1591.

[45] Y.-H. Zhang, C. K. Chan, J. F. Porter and W. Guo, Micro-Raman Spectroscopic Characterization of Nanosized TiO2 Powders Prepared by Vapor Hydrolysis, *Journal of Materials Research*, 13(2011), No.9, p.2602.

[46] T. Ohsaka, F. Izumi and Y. Fujiki, Raman spectrum of anatase, TiO2, *Journal of Raman Spectroscopy*, 7(1978), No.6, p.321.

[47] E. O. Huffman, W. E. Cate, M. E. Deming and K. L. Elmore, Solubility of Phosphates, Rates of Solution of Calcium Phosphates in Phosphoric Acid Solutions, *Journal of Agricultural and Food Chemistry*, 5(1957), No.4, p.266.

[48] W. E. Cate and M. E. Deming, Effect of impurities on density and viscosity of simulated wet-process phosphoric acid, *Journal of Chemical & Engineering Data*, 15(1970), No.2, p.290.

[49] A. Hagfeldt and M. Graetzel, Light-Induced Redox Reactions in Nanocrystalline Systems, *Chemical Reviews*, 95(1995), No.1, p.49.

[50] J. Zhang, P. Zhou, J. Liu and J. Yu, New understanding of the difference of photocatalytic activity among anatase, rutile and brookite TiO2, *Physical Chemistry Chemical Physics*, 16(2014), No.38, p.20382.

[51] N. Serpone, Is the Band Gap of Pristine TiO2 Narrowed by Anion- and Cation-Doping of Titanium Dioxide in Second-Generation Photocatalysts?, *The Journal of Physical Chemistry B*, 110(2006), No.48, p.24287.

[52] K. Madhusudan Reddy, S. V. Manorama and A. Ramachandra Reddy, Bandgap studies on anatase titanium dioxide nanoparticles, *Materials Chemistry and Physics*, 78(2003), No.1, p.239.

[53] E. M. Samsudin and S. B. Abd Hamid, Effect of band gap engineering in anionic-doped TiO2 photocatalyst, *Applied Surface Science*, 391(2017), p.326.

[54] M. Karbassi, A. Nemati, M. H. zari and K. Ahadi, Effect of Iron Oxide and Silica Doping on Microstructure, Bandgap and Photocatalytic Properties of Titania by Water-in-Oil Microemulsion Technique, *Transactions of the Indian Ceramic Society*, 70(2011), No.4, p.227.

[55] J. Schneider, M. Matsuoka, M. Takeuchi, J. Zhang, Y. Horiuchi, M. Anpo and D. W. Bahnemann, Understanding TiO2 Photocatalysis: Mechanisms and Materials, *Chemical Reviews*, 114(2014), No.19, p.9919.

[56] S. G. Kumar and L. G. Devi, Review on Modified TiO2 Photocatalysis under UV/Visible Light: Selected Results and Related Mechanisms on Interfacial Charge Carrier Transfer Dynamics, *The Journal of Physical Chemistry A*, 115(2011), No.46, p.13211.

[57] C. S. Turchi and D. F. Ollis, Photocatalytic degradation of organic water contaminants: Mechanisms involving hydroxyl radical attack, *Journal of Catalysis*, 122(1990), No.1, p.178.

[58] C. Naccache, P. Meriaudeau, M. Che and A. J. Tench, Identification of oxygen species adsorbed on reduced titanium dioxide, *Transactions of the Faraday Society*, 67(1971), No.0, p.506.

[59] W. Z. Tang and A. Huren, UV/TiO2 photocatalytic oxidation of commercial dyes in aqueous solutions, *Chemosphere*, 31(1995), No.9, p.4157.

[60] J. He,Y. Du,Y. Bai, J. An, X. Cai, Y. Chen, P. Wang, X. Yang and Q. Feng, Facile Formation of Anatase/Rutile TiO2 Nanocomposites with Enhanced Photocatalytic Activity, Molecules, 16(2019), No.24, p.2996.

[61] T. Luttrell, S. Halpegamage, J. Tao, A. Kramer, E. Sutter and M. Batzill, Why is anatase a better photocatalyst than rutile? - Model studies on epitaxial TiO2 films, *Scientific Reports*, 4(2014), p.4043.